J|A|C|S ARTICLES

Published on Web 03/30/2009

Formation of High-Quality I−III−VI Semiconductor Nanocrystals by Tuning Relative Reactivity of Cationic Precursors

Renguo Xie, Michael Rutherford, and Xiaogang Peng*

Department of Chemistry and Biochemistry, University of Arkansas, Fayetteville, Arkansas 72701

Received January 23, 2009; E-mail: renguoxie@yahoo.com; xpeng@uark.edu

Abstract: A method for the synthesis of nearly monodisperse $CuInS_2$ semiconductor nanocrystals (from <2 to 20 nm) was developed using generic and air-stable chemicals in a non-coordinating solvent. Such "greener" approaches also allowed the reaction temperatures to be below 200 °C. By introducing reactivity-controlling ligands for Cu, namely thiols, control of the Cu:In stoichiometric ratio in the nanocrystals was achieved. Amines were identified as catalytic reagents for the rapid oxidation of the $CuInS_2$ nanocrystals, which could be prevented by the formation of $CuInS_2$/ZnS core/shell nanocrystals by a one-pot approach. $CuInS_2$/ZnS core/shell nanocrystals also showed greatly improved optical properties, with photoluminescence quantum yield up to about 30% and an emission peak position tunable from 500 to 950 nm. The versatility of the synthetic strategy was demonstrated by extending it to the synthesis of $AgInS_2$ nanocrystals by simply replacing the copper salt by a silver salt.

Introduction

$CuInS_2$ and some other I−III−VI bulk crystals are direct band gap semiconductors, with a band gap of 1.45 eV for $CuInS_2$.[1] This means that it would be possible to develop color-tunable $CuInS_2$ nanocrystal emitters from the visible to near-infrared (NIR) regions with high extinction coefficients. In comparison to the current workhorse of semiconductor nanocrystal emitters, those made from CdSe, $CuInS_2$ nanocrystals should cover a broad color window, including the NIR window that is of most interest for in vivo biomedical imaging using semiconductor nanocrystal emitters.[2] Furthermore, $CuInS_2$ nanocrystal emitters are more acceptable for real-world applications because, in contrast to the CdSe-based ones, $CuInS_2$ does not contain any Class A element (Cd, Pb, and Hg) or Class B element (Se and As).

I−III−VI semiconductors, such as $CuInS_2$, are important players in photovoltaic devices as well.[3−5] Even though such photovoltaic devices are known to be less expensive in comparison to the other types of solar cells fabricated through molecular beam epitaxy and related techniques, their cost is still a major roadblock for these solar cells to compete with fossil fuels. There are two interesting ways to substantially decrease the fabrication cost at present. The first one is to explore new means to deposit high-quality semiconductor thin films, such as solution-based deposition techniques using the corresponding nanocrystals as precursors.[6] The second route aims to develop a new generation of devices, i.e., nanoengineered heterojunctions using semiconductor nanocrystals.[7−10] For both approaches, single-crystalline and nearly monodisperse semiconductor nanocrystals with tunable sizes are critical. For example, there has been substantial exploration of nanoengineered heterojunction solar cells using well-developed CdSe and other semiconductor nanocrystals,[7,11] although the intrinsic toxicity of elemental cadmium is an apparent environmental concern. Conversely, there has been barely any investigation into using $CuInS_2$ nanocrystals for such a new generation of devices, presumably due to the poor quality of $CuInS_2$ nanocrystals.

InP and InAs nanocrystals as representative III−V semiconductor nanocrystals, which at least do not have Class A elements as a component, may compete with $CuInS_2$ dots both for solar cell fabrication and as nanocrystals emitters. Our recent progress[12−14] on synthesis of such nanocrystals brought the quality of these nanocrystals, especially their emissive properties, up to a level comparable to that of CdSe and II−VI semicon-

(1) Klenk, R.; Blieske, U.; Dieterle, V.; Ellmer, K.; Fiechter, S.; Hengel, I.; JagerWaldau, A.; Kampschulte, T.; Kaufmann, C.; Klaer, J.; LuxSteiner, M.; Braunger, D.; Hariskos, D.; Ruckh, M.; Schock, H. W. *Sol. Energy Mater. Sol. Cells* **1997**, *49*, 349.
(2) Michalet, X.; Pinaud, F. F.; Bentolila, L. A.; Tsay, J. M.; Doose, S.; Li, J. J.; Sundarensan, G.; Wu, A. M.; Gambhir, S. S.; Weiss, S. *Science* **2005**, *307*, 538.
(3) Bailey, S. G.; Flood, D. *J. Prog. PhotovoltaicRes. Appl.* **1998**, *6*, 1.
(4) Raffaelle, R. P.; Castro, S. L.; Hepp, A. F.; Bailey, S. G. *Prog. Photovoltaics* **2002**, *10*, 433.
(5) Nanu, M.; Schoonman, J.; Goossens, A. *Nano Lett.* **2005**, *5*, 1716.
(6) Panthani, M. G.; Akhavan, V.; Goodfellow, B.; Schmidtke, J. P.; Dunn, L.; Dodabalapur, A.; Barbara, P. F.; Korgel, B. A. *J. Am. Chem. Soc.* **2008**, *130*, 16770.
(7) Greenham, N. C.; Peng, X. G.; Alivisatos, A. P. *Phys. Rev. B* **1996**, *54*, 17628.
(8) Wu, Y. Y.; Fan, R.; Yang, P. D. *Nano Lett.* **2002**, *2*, 83.
(9) Peng, H. L.; Xie, C.; Schoen, D. T.; Mcllwrath, K.; Zhang, X. F.; Cui, Y. *Nano Lett.* **2007**, *7*, 3734.
(10) Kamat, P. V. *J. Phys. Chem. C* **2007**, *111*, 2834.
(11) Huynh, W. U.; Dittmer, J. J.; Alivisatos, A. P. *Science* **2002**, *295*, 2425.
(12) Xie, R. G.; Battaglia, D.; Peng, X. G. *J. Am. Chem. Soc.* **2007**, *129*, 15432.
(13) Xie, R. G.; Peng, X. G. *Angew. Chem., Int. Ed.* **2008**, *47*, 7677.
(14) Xie, R. G.; Chen, K.; Chen, X. Y.; Peng, X. *Nano Res.* **2008**, *1*, 457.

ductor nanocrystals.[15,16] From a green chemistry viewpoint, unfortunately, these III−V semiconductor nanocrystals were obtained by using extremely expensive, unstable, hazard precursors, such as tris-trimethylsily phosphide and tris-trimethylsilyl arsenide. Another point which is worth mentioning is the poor chemical stability of phosphides and arsenides in comparison to sulfides, which is always a concern in technical applications.

An obvious challenge for synthetic chemistry of I−III−VI semiconductors nanocrystals is their ternary composition, instead of the binary composition of the common II−VI and III−V semiconductor nanocrystals. As a result, the stoichiometric ratio between the Group I and Group III elements of a nanocrystal may vary substantially in a given sample with either cubic or wurzite crystal structure.[17] Not surprisingly, synthesis of I−III−VI semiconductor nanocrystals, such as $CuInS_2$, is not a new topic in the field of colloidal nanocrystals. Several independent methods have been reported for their synthesis, such as solid-phase synthesis,[18,19] hydrothermal techniques,[20−23] single-source precursor routes,[24−26] and hot injection techniques.[6,17,27−31] In comparison to the overall quality of binary semiconductor nanocrystals reported in literature,[15,16] the size and size distribution control, tenability in size, and/or optical properties of I−III−VI ternary nanocrystals are much less developed.

This work intended to explore controlled synthesis of $CuInS_2$ nanocrystals using "greener" approaches as an example for synthesis of ternary compound semiconductor nanocrystals with a controlled stoichiometric ratio between three elements. In light of the importance of the precursor ratio in controlling the optical properties of semiconductor nanocrystals, we decided to develop the synthetic chemistry using three independent precursors for the three components: indium fatty acid salts, copper acetate (with thiols as the reactivity controller), and sulfur powder. The key for the successful synthesis of nearly monodisperse $CuInS_2$ nanocrystals in a reasonably large size range, from <2 to 20 nm, was to balance the reactivity of the two cationic precursors by their ligands, solution composition, and reaction temperature. To improve their performance as emissive materials, methods were also developed for the introduction of a ZnS shell around the $CuInS_2$ nanocrystals in a one-pot fashion. Some preliminary results on the synthesis of $AgInS_2$ nanocrystals are also reported to demonstrate the general applicability of the synthetic chemistry.

Results and Discussion

Balancing the reactivity of two cationic precursors was found to be the key to the successful development of the synthetic scheme for the targeted ternary compound nanocrystals, those of $CuInS_2$ and $AgInS_2$. In recent years, metal fatty acid salts have been used predominantly as precursors for synthesis of high-quality nanocrystals involving metal components in organic solvents because of their stability, wide availability for nearly all metal elements, relatively low toxicity, and inexpensive nature. When indium and copper carboxylates were used as the precursors, however, formation of Cu_xS ($x = 1-2$) nanophases (see Figure S1, Supporting Information) was found to be inevitable when the solution was composed of pure non-coordinating solvent (such as octadecene, ODE), trioctylphosphine oxide (TOPO), amines, carboxylic acid, and their mixtures, even if the reaction temperature was so low that indium sulfide would not form under the given conditions. This indicates that copper fatty acid salts were too reactive in comparison to indium fatty acid salts in these reaction media. One simple way to suppress the reactivity of metal fatty acid salts as precursors for formation of high-quality colloidal nanocrystals in nonaqueous phases is to add a high concentration of free fatty acids.[12,32] However, this strategy also did not prevent the formation of Cu_xS nanophases.

Considering that Cu^+ ions are very soft Lewis acids, we suspected that the hard Lewis base ligands (fatty acids) might not be good ligands to suppress the reactivity of the copper ions. It was noticed that thiols were used as the ligands for I−III−VI semiconductor nanocrystals previously, although the resulting nanocrystals did not possess good size distribution.[24] For this reason, we chose soft Lewis base ligands for copper ions, alkane thiols. Though the thiol ligands made copper much less reactive, the reaction temperature should be controlled under 230 °C. Our control experiments and reports from other research groups[33,34] revealed that copper thiolate in nonaqueous solution could decompose into Cu_xS nanophases at reaction temperatures above 230 °C. Although our results shall further reveal that this could be overcome by using a large excess of thiols, a substantially high thiol concentration may cause some other complications, as will be discussed below. Fortunately, indium fatty acid salts also had a similar temperature, limit as reported previously,[35,36] because of their hydrolysis at elevated temperatures.

The chemical composition of the resulting nanocrystals was determined mainly by energy-dispersive spectroscopy (EDX) (Figure 1A). The composition of the resulting nanocrystals was

(15) Murray, C. B.; Norris, D. J.; Bawendi, M. G. *J. Am. Chem. Soc.* **1993**, *115*, 8706.
(16) Peng, Z. A.; Peng, X. *J. Am. Chem. Soc.* **2001**, *123*, 183.
(17) Pan, D. C.; An, L. J.; Sun, Z. M.; Hou, W.; Yang, Y.; Yang, Z. Z.; Lu, Y. F. *J. Am. Chem. Soc.* **2008**, *130*, 5620.
(18) Yoshino, K.; Ikari, T.; Shirakata, S.; Miyake, H.; Hiramatsu, K. *Appl. Phys. Lett.* **2001**, *78*, 742.
(19) Torimoto, T.; Adachi, T.; Okazaki, K. i.; Sakuraoka, M.; Shibayama, T.; Ohtani, B.; Kudo, A.; Kuwabata, S. *J. Am. Chem. Soc.* **2007**, *129*, 12388.
(20) Jiang, Y.; Wu, Y.; Mo, X.; Yu, W. C.; Xie, Y.; Qian, Y. T. *Inorg. Chem.* **2000**, *39*, 2964.
(21) Lu, Q. Y.; Hu, J. Q.; Tang, K. B.; Qian, Y. T.; Zhou, G. E.; Liu, X. M. *Inorg. Chem.* **2000**, *39*, 1606.
(22) Xiao, J.; Xie, Y.; Xiong, Y.; Tang, R.; Qian, Y. T. *J. Mater. Chem.* **2001**, *11*, 1417.
(23) Ahn, S.; Kim, K. H.; Chun, Y. G.; Yoon, K. G. *Thin Solid Films* **2007**, *515*, 4036.
(24) Castro, S. L.; Bailey, S. G.; Banger, K. K.; Hepp, A. F. *Chem. Mater.* **2003**, *15*, 3142.
(25) Castro, S. L.; Bailey, S. G.; Banger, K., K.; Hepp, A. F. *J. Phys. Chem. B* **2004**, *108*, 12429.
(26) Nairn, J. J.; Schapiro, P. J.; Twamley, B.; Pounds, T.; Wandruszka, R. V.; Williams, M.; Wang, C. M.; Notton, M. G. *Nano Lett.* **2006**, *6*, 1218.
(27) Malik, M. A.; O'Brien, P.; Revaprasadu, N. *Adv. Mater.* **1999**, *11*, 1441.
(28) Czekelius, C.; Hilgendorff, M.; Spanhel, L.; Bedja, I.; Lerch, M.; Muller, G.; Bloeck, U.; Su, D. S.; Giersig, M. *Adv. Mater.* **1999**, *11*, 643.
(29) Nakamura, H.; Kato, W.; Uehara, M.; Nose, K.; Omata, T.; Matsuo, O., S.; Miyazaki, M.; Maeda, H. *Chem. Mater.* **2006**, *18*, 3330.
(30) Zhong, H. Z.; Zhou, Y.; Ye, M. F.; He, Y. J.; Ye, J. P.; He, C.; Yang, C. H.; Li, Y. F. *Chem. Mater.* **2008**, *20*, 6434.
(31) Arici, E.; Sariciftci, N. S.; Meissner, D. *Adv. Funct. Mater.* **2003**, *13*, 165.
(32) Yu, W. W.; Wang, Y. A.; Peng, X. *Chem. Mater.* **2003**, *15*, 4300.
(33) Sigman, M. B.; Ghezelbash, A.; Hanrath, T.; Saunders, A. E.; Lee, F.; Korgel, B. A. *J. Am. Chem. Soc.* **2003**, *125*, 16050.
(34) Lim, W. P.; Wong, C. T.; Ang, S. L.; Low, H. Y.; Chin, W. S. *Chem. Mater.* **2006**, *18*, 6170.
(35) Battaglia, D.; Peng, X. G. *Nano Lett.* **2002**, *2*, 1027.
(36) Narayanaswamy, A.; Xu, H.; Pradhan, N.; Kim, M.; Peng, X. *J. Am. Chem. Soc.* **2006**, *128*, 10310.

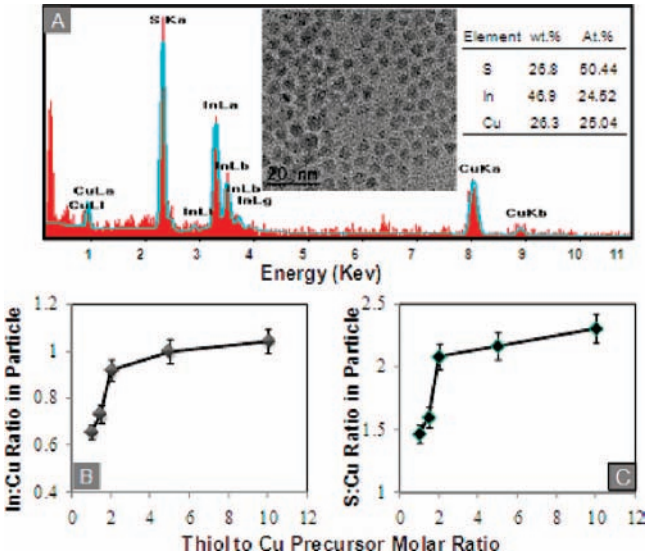

Figure 1. (A) EDX spectrum of nanocrystal sample. Insets: TEM view of the particles for EDX measurement and the quantitative elemental analysis results. (B) In:Cu ratio and (C) S:Cu ratio of the nanocrystals versus the thiol concentration.

found to be strongly dependent on the thiol concentration, and this dependence can be clearly divided into two regions (Figure 1B,C). If the initial thiol-to-copper molar ratio was smaller than 2:1, the EDX results revealed that both In:Cu and S:Cu ratios increased rapidly, but the nanocrystals were still copper-rich in comparison to the stoichiometry of $CuInS_2$. However, at a thiol-to-copper ratio higher than 2:1, the Cu:In ratio of the nanocrystals determined by EDX was consistent with that expected from the $CuInS_2$ structure within experimental error. The In:Cu ratio of the samples was also determined by atomic absorption (AA) (Figure S2, Supporting Information) and was consistent with the EDX values. Unfortunately, limited by the detection sensitivity, AA could not reliably determine the concentration of S in a sample.

The S:Cu ratio of the nanocrystals (Figure 1C) was found to be slightly higher than expected for $CuInS_2$. This was probably due to some of the thiol ligands bonding onto the surface of the nanocrystals. This hypothesis could be supported by a surface ligand exchange experiment. It has been reported repeatedly that mercaptopropanoic acid (MPA) could replace both fatty acid and fatty amine ligands of the semiconductor nanocrystals to make those particles water-soluble.[12−14] In principle, the thiol group of MPA was a relatively strong anchoring groups for the surface cationic sites on those nanocrystals in comparison to the original ligands. However, this ligand-exchange strategy did not work for the $CuInS_2$ nanocrystals obtained with thiol ligands.

The above facts indicate that the minimum amount of thiol ligands needed to warrant a desired reactivity of the copper precursor for the formation of $CuInS_2$ with the expected stoichiometry was about 2:1, which means two thiol molecules per copper ion. It should be mentioned that, although the nanocrystals mentioned in this work sometimes did not have this exact stoichiometry of $CuInS_2$, we refer them as $CuInS_2$ for simplicity.

The absorption band edge of the resulting nanocrystals was found to be strongly dependent on the thiol concentration, with the other reaction conditions being constant when the thiol-to-copper acetate ratio was below about 3:1 (Figure 2A). Part of the reasons should be the composition variation with a relatively low thiol concentration discussed in the above

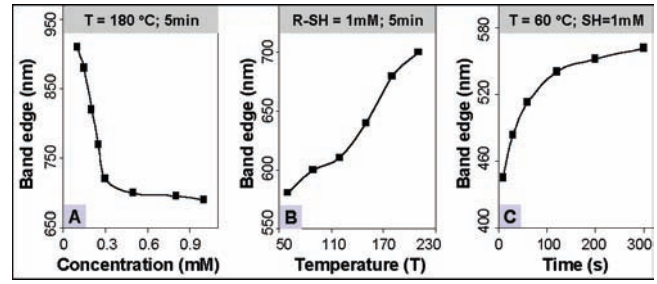

Figure 2. Temporal evolution of UV−vis−NIR absorption band edge of $CuInS_2$ nanocrystals with varying thiol concentration (A), reaction temperature (B), and reaction time (C). The copper acetate concentration in all these reactions was maintained as 0.1 mmol/L (mM).

paragraph. With the increase of the copper content in $CuIn_xS_{((1+3x)/2)}$, the bandgap of the semiconductor should decrease,[37] implying a significant red-shift of the bulk absorption band edge.

The absorption band edge of the resulting nanocrystals was found to depend on the reaction temperature and reaction time as well whether the initial thiol-to-copper ratio was fixed (Figure 2B,C). However, it should be pointed out that, for some reaction temperatures (below 120 °C), a relatively large excess of thiol (at least 2 times the number of copper ions in the initial mixture) would be needed to avoid the formation of pure Cu_2S nanophases that could be identified by electron diffraction (see Figure S1). For a high-temperature reaction, the minimum thiol:Cu ratio could be as low as 1:1. This was likely due to the low reactivity of indium fatty acid salts under low temperatures. As a result, more thiols were needed to further reduce the reactivity of the copper ions.

Figure 2C shows that, when the reaction temperature was set at 60 °C, the absorption band edge of the as-synthesized nanocrystals shifted from ~450 to ~570 nm as the reaction time increased from 10 to 300 s. However, the degree of red-shift of the absorption edge depended on the reaction temperature. Detailed studies revealed that the absorption spectra of the nanocrystals were almost constant from the starting point—the injection of the sulfur precursor solution—to about an hour of heating if the reaction temperature was 180 °C or higher. However, the results in Figure 2B indicate that the high-temperature reaction actually yielded substantially large particles, judged by the significantly red-shifted absorption band edge (comparing the absorption band edge position for the reaction at 180 °C to that at 60 °C). This result excluded the possibility that the nucleation process consumed all monomers in the solution needed for the following growth process, which would otherwise yield very small particles. In combination, all these results suggest that a plausible explanation for this interesting temperature-dependent growth pattern would be the thermally enhanced reactivity of the precursors. As a result, soon after the nucleation process, the growth of the nuclei was greatly enhanced at a relatively high temperature, which yielded large nanocrystals in a very short time frame.

It should be pointed out that, at low reaction temperatures (between 60 and 150 °C), the sulfur precursor solution must contain some alkylamines to activate the reaction, presumably the indium fatty acid salts.[12] For the high temperatures, the reaction system did not need to have amines. Even with the amines in the reaction mixture, growth of $CuInS_2$ nanocrystals

(37) Nair, M. T. S.; Guerrero, L.; Nair, P. K. *Semicond. Sci. Technol.* **1998**, *13*, 1164.

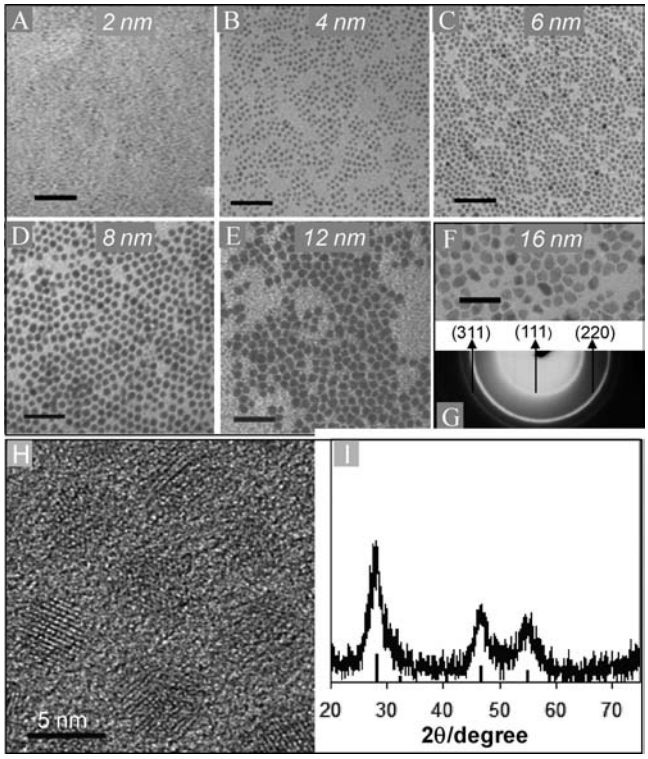

Figure 3. (Top) TEM pictures and a representative ED pattern of $InCuS_2$ nanocrystals. The scale is 50 nm. (Bottom) HR-TEM image and XRD pattern of one sample of $CuInS_2$ nanocrystals.

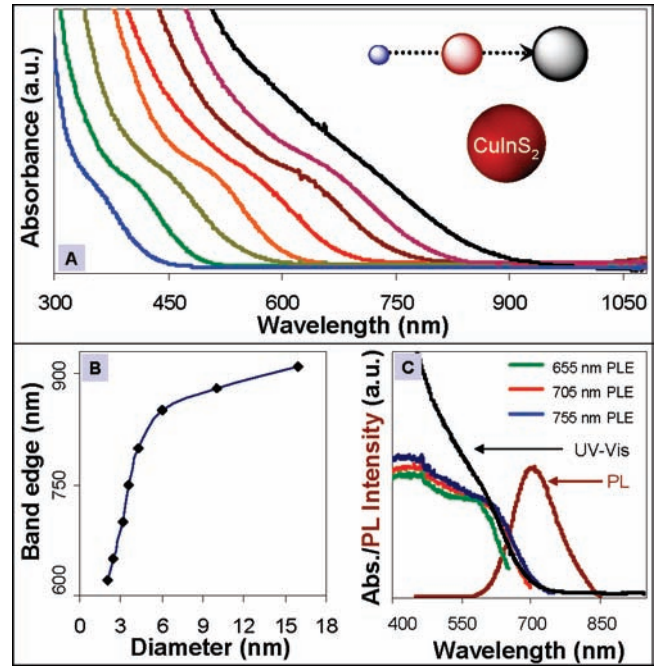

Figure 4. (A) Absorption spectra of different-sized $InCuS_2$ nanocrystals, (B) the size-dependent absorption band edge, (C) and the position-dependent photoluminescence excitation (PLE) spectra.

was not feasible if the reaction temperature was below 60 °C. As will be discussed below, the excess amines in the reaction mixture must be removed to maintain the stability of the plain core $CuInS_2$ nanocrystals.

Control over the size, size distribution, shape, and crystallinity of the copper indium sulfide nanocrystals was achieved using the current strategy (Figure 3). When the sizes were smaller than 5 nm, the nearly monodisperse nanocrystals were obtained directly from synthesis. For the larger ones in Figure 3C,D, size-selective precipitation was applied to further narrow-down the size distribution. The transmission electron microscopy (TEM) pictures show that the small nanocrystals (<10 nm) were mostly spherical, and the relatively large ones possessed a somewhat faceted shape. The nanocrystals shown in Figure 3 all had similar diffraction patterns (Figure 3G,I), which indicates a cubic structure,[17] although the composition of the nanocrystals varied somewhat, as discussed above.

The single-crystalline nature of the resulting nanocrystals was revealed by high-resolution TEM (HR-TEM) experiments, evidenced by the continuous lattice fringes throughout each particle (Figure 3H). The phase purity of the cubic structure of the nanocrystals was further confirmed by powder X-ray diffraction (XRD) (Figure 3I). The crystal domain size, determined on the basis of the peak widths in the XRD pattern using the Scherrer equation, was consistent with the average particle sizes determined by TEM measurements.

The absorption and emission properties of the $CuInS_2$ nanocrystals showed the expected blue-shift upon decreasing the size of the nanocrystals (Figure 4A). Because there was no apparent absorption peak, the absorption band edge was used to relate the size of the nanocrystals with the absorption properties of the nanocrystals (Figure 4B). It was difficult to accurately measure nanocrystals smaller than about 2 nm because of the limits of the experimental techniques; thus, data points with their absorption edge below about 600 nm are not shown in Figure 4B. The trend of the size dependence of the absorption edge shown in Figure 4B indicates that the red-shift of the absorption spectra of the $CuInS_2$ nanocrystals became not very significant for nanocrystals larger than about 10 nm.

To the best of our knowledge, the absorption spectra of $CuInS_2$ and other I−III−VI nanocrystals typically did not show well-defined exciton absorption peaks.[25,30] The special electronic properties in comparison to II−VI semiconductor nanocrystals were considered as one possible reason.[1,7] The second possible reason could be the iregular composition distribution among different nanocrystals in an ensemble. The third possibility would be the standard issue for quantum confinement semiconductor nanocrystals, that is, the size/shape inhomogeneity of the ensemble. For the nanocrystals presented in this report, the last one seems to be the answer.

As shown in Figure 4C, the photoluminescnece excitation (PLE) spectra of a given sample at different emission positions reveal a substantial dependence on the emission position for monitoring the PLE. As shown in Figure 4C, the PLE spectra systematically shifted to blue as the emission possition for monitoring the PLE spectra shifted to blue. Furthermore, the PLE at the short wavelength showed a reasonably well-defined exciton peak, which is expected for PLE line narrowing at the short-wavelength side of the PL peak.[15] This evidence indicates that the broad absorption spectra shown in Figure 4A were largely due to the size/shape inhomogeneity.

To further confirm the above hypothesis, some careful size-selective precipitaiton was performed to narrow down the size distribution of the nanocrystals. Size-selective precipitation was performed for $CuInS_2$/ZnS core/shell nanocrystals with one monolayer of ZnS shell because of their impoved PL properties and stability. After the size-selective precipitation, TEM measurements for small sizes often did not show substantial improvement. Accordingly, however, the UV−vis spectrum

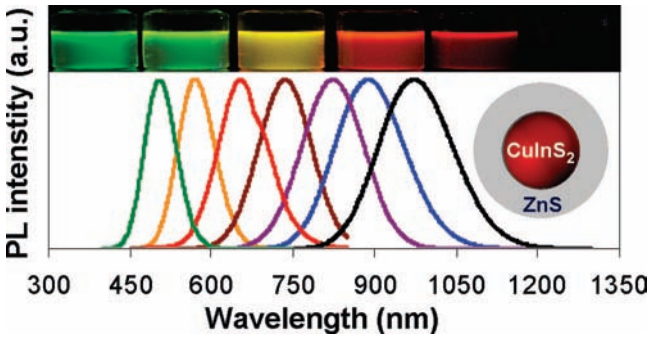

Figure 5. Photoluminescence properties of the $CuInS_2$/ZnS core/shell nanocrystals.

became sharpened, and a well-defined excitonic absorption peak could be identified (Figure S3, Supporting Information). Nevertheless, the nature of the broad emission peak was completely retained before and after the size selection (Figure S3), although the PLE spectra match well with absorption spectra for the samples after the size sorting. These results strongly support the conclusion drawn in the above paragraph, and the broad PL seems to be consistent with the "donor−acceptor pair" model suggested by Krustok et al.[38,39]and the "Shockley, Read, and Hall recombination" model reported by Hofhuis et al.[40]

One-pot synthesis of $CuInS_2$/ZnS core/shell nanocrystals was developed for the $CuInS_2$ nanocrystals grown using the scheme described above. To avoid the formation of separate ZnS nanoparticles, a succesive ion layer adsorption and reaction (SILAR) technique[41,42] coupled with thermal cycling[43] was adopted for the growth of the core/shell nanocrystals, i.e., at about 80 °C for the injection of the shell precursors and 210 °C for the growth of the shell materials (see details in Experimental Section). Upon the growth of the core/shell nanocrystals, an apparent increase in size of the nanocrystals was identified using TEM.

The growth of core/shell nanocrystals improved the emission properties substantially, although it did not affect the absorption spectra significantly. Before the growth of the ZnS shell, the $CuInS_2$ plain core nanocrystals did show bandgap emission but with quite low PL quantum yield, typically below 3%. After the ZnS shell growth, the PL properties of the resulting core/shell nanocrystals became qutie good. Without substantial optimization, the PL quantum yield increased about 10 times and reached close to 30%. The emission color of the $CuInS_2$ nanoparticles covered a broad window (from about 500 to 950 nm), the most part of the visible window and a significant portion of the near-infrared window that is relevant to in vivo imiging (Figure 5).

The growth of core/shell nanocrystals improved not only the PL brightness of the $CuInS_2$ nanocrytals but also their chemical/photochemical stability. Although synthesis of $CuInS_2$ or other types of I−III−VI semiconductor nanocrystals has been explored intensively recently, to our knowledge, there is no report on studying their chemical stability. Our studies revealed an interesting stability feature of the $CuInS_2$ nanocrystals. As shown in Figure 6A, the plain core nanocrystals were reasonably stable in solution under ambient conditions if no amines were presented in the solution. However, if there were amines in the solution, the absorption spectrum of the nanocrystals would blue-shift quite rapidly (Figure 6B) under the same conditions, indicating the shrinkage of the $CuInS_2$ core. By monitoring the PL properties, it was identified that the PL brightness decreased gradually along with the shrinkage of the size of the nanocrystals (Figure 6C).

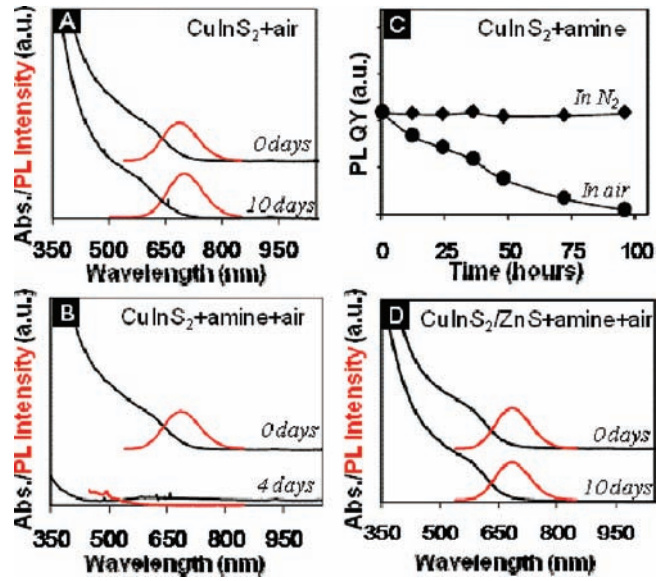

Figure 6. Stability of $CuInS_2$ core and $CuInS_2$/ZnS core/shell nanocrystals.

Although it was suspected that amines could etch CdSe nanocrystals,[44] the shrinkage observed here for $CuInS_2$ nanocrystals was not an etching process. As shown in Figure 6C, if no air was present, the $CuInS_2$ core nanocrystals were actually stable upon aging. In addition, amines either from the reaction mixture or added after synthesis all showed the same effects. These results indicate that the amines were catalytic reagents in the oxidation of the core nanocrystals that was in turn responsible for the observed blue-shift of the optical spectra and the decrease of PL brightness in Figure 6B,C.

Growth of the ZnS shell made the $CuInS_2$ nanocrystals stable under all conditions tested. As shown in Figure 6D, a solution of the core/shell nanocrystals was examined with both amine and air in place, and no detectable changes were observed by optical measurements. The results in Figure 6D show the data for only 10 days, but further measurements showed that the $CuInS_2$/ZnS core/shell nanocrystals could actually be stable for at least several months under the testing conditions. These results are consistent with a $CuInS_2$/ZnS core/shell nanocrystal structure with a complete coating of a ZnS shell.

$AgInS_2$ nanocrystals were also synthesized using the same technique, tuning the reactivity of the Group IB metal ions by thiol ligands. Essentially, the difference between the syntheses of $CuInS_2$ and $AgInS_2$ nanocrystals was only the precursor of the Group IB metal, silver nitride instead of copper(I) acetate.

(38) Krustok, J.; Schon, J. H.; Collan, H.; Yakushev, M.; Madasson, J.; Bucher, E. *J. Appl. Phys.* **1996**, *86*, 364.
(39) Krustok, J.; Raudoja, J.; Schon, J. H.; Yakushev, M.; Collan, H. *Thin Solid Films* **2000**, *361*, 406.
(40) Hofhuis, J.; Schoonman, J.; Goossens, A. *J. Phys. Chem. C* **2008**, *112*, 15052.
(41) Li, J. J.; Wang, Y. A.; Guo, W. Z.; Keay, J. C.; Mishima, T. D.; Johnson, M. B.; Peng, X. G. *J. Am. Chem. Soc.* **2003**, *125*, 12567.
(42) Xie, R.; Kolb, U.; Li, J.; Basche, T.; Mews, A. *J. Am. Chem. Soc.* **2005**, *127*, 7480.
(43) Blackman, B.; Battaglia, D. M.; Mishima, T. D.; Johnson, M. B.; Peng, X. G. *Chem. Mater.* **2007**, *19*, 3815.
(44) Li, R. F.; Lee, J.; Yang, B. C.; Horspool, D. N.; Aindow, M.; Papadimitrakopoulos, F. *J. Am. Chem. Soc.* **2005**, *127*, 2524.

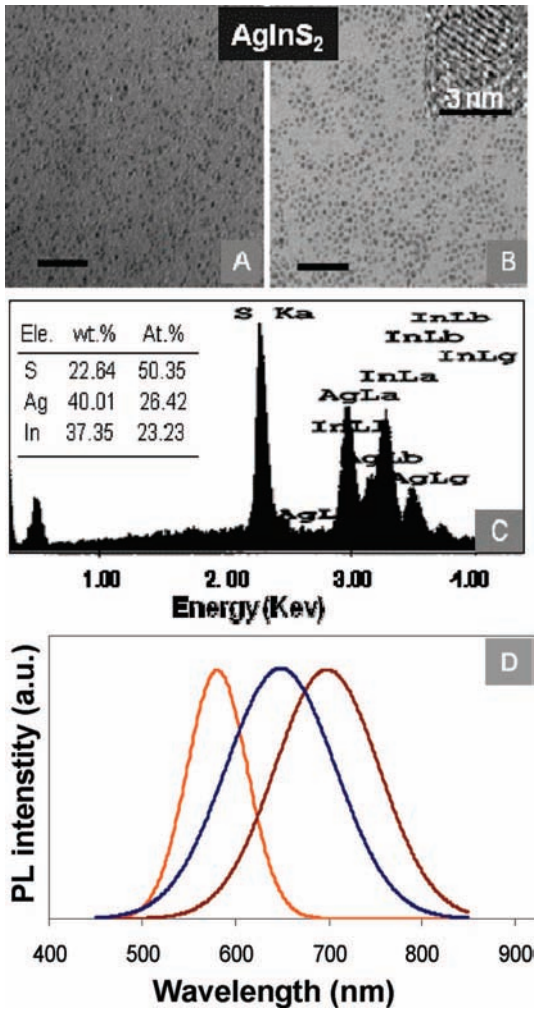

Figure 7. (A,B) TEM, (C) EDX, and HR-TEM images (inset in B) of $AgInS_2$ nanocrystals. The scale bar is 50 nm. (D) Examples of their PL spectra are also shown.

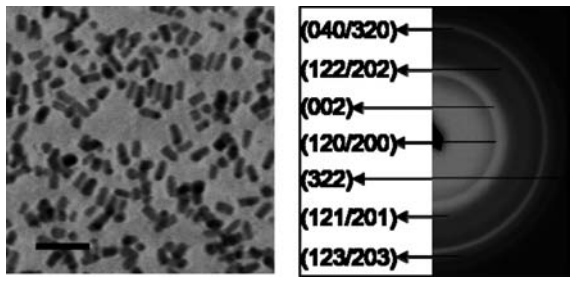

Figure 8. (A) TEM image of $AgInS_2$ nanorods and (B) electron diffraction pattern of as-prepared $AgInS_2$ nanocrystals. The scale bar is 50 nm.

The preliminary results revealed that the size of the resulting $AgInS_2$ nanocrystals could be effectively tuned from ~2 nm to over 10 nm. The as-synthesized $AgInS_2$ nanocrystals possessed a narrow size distribution, shown by TEM measurements (Figure 7A,B). The lattice fringes were clearly observed in the HR-TEM (Figure 7B inset), which indicates the high crystallinity of these nanocrystals. The crystal structure of the $AgInS_2$ nanocrystals determined by the diffraction methods (see Figure 8B as an example) was identified as orthorhombic $AgInS_2$ (JCPDS 00-025-1328). The composition of the nanocrystals determined by the EDX technique (Figure 7C) was found to be the same as that for the $AgInS_2$ phase within experimental error. Although there is no report on band gap PL of $AgInS_2$ nanocrystals, the nanocrystals synthesized through our approach showed pure band gap emission. The PL quantum yield of the as-synthesized $AgInS_2$ nanocrystals was found to be ~8%, and the PL peak could be tuned from 570 to 720 nm by our preliminary efforts (Figure 7D).

Formation of rod shaped $AgInS_2$ nanocrystals was also realized via this simple synthetic route (Figure 8). The key parameter for the controlled formation of $AgInS_2$ nanorods was a low reaction temperature, ~below 100 °C. According to the current understanding of formation of elongated nanocrystals,[45] a low temperature would enable formation of a small amount of nuclei. Subsequently, the residual monomer concentration in the solution would be high. This means a high chemical environment needed for the growth of the elongated nanocrystals.

Conclusion

In summary, we have developed a "greener" method for synthesis of high-quality $CuInS_2$ nanocrystals in the size range between about 2 and 20 nm by adjusting the relative reactivity of Cu precursor vs indium precursor in a non-coordinating solvent. The copper-to-indium ratio in this ternary compound was successfully controlled by this strategy. In comparison to the synthesis of binary compound semiconductor nanocrystals, such a reaction system was found to be much more sensitive to the reaction solution composition, reaction temperature, and reaction time. The $CuInS_2$ nanocrystals were found to be substantially more sensitive to oxidation with the presence of amines, but this stability problem was solved by coating the nanocrystals with a ZnS shell. The formation of $CuInS_2$/ZnS core/shell nanocrystals further improved the photoluminescence quantum yield by about 10 times, up to about 30%, with the emission peak position covering most of the visible and NIR window. The results revealed that the nature of the broad absorption spectra that have been universally observed for I−III−VI semiconductor nanocrystals is likely due to the size/shape inhomogenity of nanocrystals, instead of the composition variation from particle to particle in an ensemble. Preliminary results on the synthesis of $AgInS_2$ nanocrystals showed that this synthetic strategy, tuning the relative reactivity of the Group IB metal precursor, is likely feasible for synthesizing other types of I−III−VI nanocrystals. This may further open a new route for the synthesis of multinary nanocrystals by controlling the relative reactivity of precursors.

Experimental Section

Materials. Technical grade (90%) octadecene (ODE), indium acetate ($In(Ac)_3$, 99.99%), tri-*n*-octylphosphine (TOP, 97%), stearic acid (SA, 98%), copper(II) acetate (99.999%), oleic acid (90%), zinc stearate (ZnO, 12.5−14%), and silver nitrate (99.9%) were purchased from Alfa. Copper(I) acetate (99.5%), oleylamine (97%), *n*-dodecylthiol (SH, 99.9%), and sulfur powder (S, 9.999%) were purchased from Aldrich. Indium stearate was prepared in our laboratory. All the chemicals were used without further purification.

Synthesis of $CuInS_2$ Nanocrystals. For a typical synthetic reaction, 0.1 mM indium stearate, 0.1 mM copper(I)/(II) acetate, 0.2 mM oleic acid, and 4 mL of ODE were loaded into a three-neck flask. This mixture was heated to 80 °C. When the solution became clear, 1 mM *n*-dodecylthiol was added into reaction solution. At this moment, the color of the solution changed from slight green (copper(I)) or slight blue (copper(II)) to slight yellow. Next, 0.3 mM sulfur dissolved in oleylamine or ODE solution was quickly

(45) Peng, Z. A.; Peng, X. G. *J. Am. Chem. Soc.* **2001**, *123*, 1389.

injected into the reaction solution at 180 °C. For low-temperature reactions (<100 °C), several drops (about 0.1 mL) of TOP were added into the reaction solution to maintain the solubility of the resulting $CuInS_2$ nanocrystals. Finally, the solution was cooled to room temperature.

In Situ Synthesis of $CuInS_2$/ZnS Core/Shell Nanocrystals. The growth solution of $CuInS_2$ quantum dots was set at 80 °C. Next, 0.1 mM zinc stearate in ODE/oleylamine (the ratio of ODE/oleylamine is 4/1, in all 0.5 mL) was injected into a reaction flask including $CuInS_2$ nanocrystals. After that, the temperature was increased to 210 °C for 30 min to allow the growth of the ZnS shell.

Synthesis of $AgInS_2$ Nanocrystals. In a typical synthetic reaction, 0.1 mM indium stearate, 0.1 mM silver nitrate, 0.1 mM oleic acid, 1 mM *n*-dodecylthiol, and 4 mL of ODE were loaded into a three-neck flask. This mixture became clear when it was heated to 90 °C. At that moment, 0.3 mM sulfur dissolved in oleylamine was quickly injected into the reaction solution, and then the temperature was set to 120 °C for growth of $CuInS_2$ nanocrystals. Finally, the solution was cooled to room temperature.

Transmission Electron Microscopy (TEM) and High-Resolution TEM (HR-TEM). The low-resolution TEM images were taken on a JEOL 100CX transmission electron microscope with an acceleration voltage of 100 kV. Carbon-coated copper grids were dipped in the hexanes or toluene solutions to deposit nanocrystals onto the film. HR-TEM pictures were taken using a Taitan microscope with an acceleration voltage of 300 kV.

X-ray Powder Diffraction (XRD). XRD patterns were obtained using a Philips PW1830 X-ray diffractometer.

Energy-Dispersive Spectroscopy (EDS). For elemental analysis, a Taitan F30ST (FEI) instrument with a field emission gun was operated at 300 kV, equipped with an EDAX spectrometer with a Si/Li detector. For comparison, ED spectra were obtained by using a Philips ESEM XL30 scanning electron microscope equipped with a field emission gun and operated at 10 kV.

Optical Measurements. UV−vis spectra were recorded on an HP8453 UV−visible spectrophotometer. Photoluminescence (PL) spectra were taken using a Spex Fluorolog-3 fluorometer. Fluorescence quantum yields were estimated by comparison of the fluorescence intensity with standard dye solutions with the same optical density at the excitation wavelength and similar fluorescence wavelength.

Atomic Absorption (AA) Measurements. A purified $CuInS_2$ nanocrystal sample was dried by gentle heating under argon, and then the sample was digested by 0.5 mL of aqua regia. The digested sample was transferred into a volumetric flask to make an aqueous solution for the AA measurement. The concentrations of copper and indium were determined using a GBC 932 atomic absorption spectrometer.

Stability Tests. The stability experiments were performed under air and N_2, respectively. The samples tested with and without amine were exposed to sunlight, respectively. UV−vis and PL spectra were measured at certain time intervals.

Acknowledgment. This work was partially supported by the NSF and NIH, and we thank Dr. M. Benamara for HR-TEM measurements.

Supporting Information Available: Characterization of as-prepared Cu_xS and $CuInS_2$/ZnS nanocrystals by TEM, EDS, UV−vis, and PL spectra. This information is available free of charge via the Internet at http://pubs.acs.org.

JA9005767